

Quantum paraelectric behavior of pyrochlore PMN

S. Kamba,* D. Nuzhnyy, S. Denisov, S. Veljko, V. Bovtun, M. Savinov, and J. Petzelt
*Institute of Physics, Academy of Sciences of the Czech Republic,
v.v.i. Na Slovance 2, 182 21 Prague 8, Czech Republic*

M. Kalnberga and A. Sternberg
*Institute of Solid State Physics, University of Latvia, Kengaraga str. 8, Riga, Latvia
(Dated: October 31, 2018)*

$\text{Pb}_{1.83}\text{Mg}_{0.29}\text{Nb}_{1.71}\text{O}_{6.39}$ (PMN) crystallizing in a cubic pyrochlore structure exhibits, as the first dielectrics with pyrochlore structure, typical feature of quantum paraelectrics - its permittivity continuously increases on cooling and levels off below ~ 30 K without any signature of a structural phase transition. Broad-band dielectric spectra do not show any dielectric dispersion in the real part of permittivity up to 8.8 GHz. THz and infrared spectra reveal a soft polar optic mode which is responsible for the temperature dependence of the permittivity. The leveling-off of the permittivity at low temperatures obeys the Barrett formula and the fitted vibrational zero-point energy $\frac{1}{2}k_B T_1$ corresponds to the measured soft mode frequency. The number of observed infrared phonons exceeds that predicted from the factor-group analysis which indicates that the structure is at least locally non-cubic.

PACS numbers: 63.20.-e; 77.22.-d; 78.30.-j; 67.20.+k

I. INTRODUCTION

$\text{PbMg}_{1/3}\text{Nb}_{2/3}\text{O}_3$ crystallizing in the cubic perovskite structure is one of the most studied dielectrics as the typical representative of relaxor ferroelectrics. It exhibits a high ($\sim 10^4$) and strongly diffused peak in the temperature dependent permittivity whose position remarkably shifts from 245 K (at 100 Hz) to 320 K (at 1 GHz).^{1,2} Its crystal structure remains cubic down to liquid He temperatures. The peculiar dielectric properties are caused by a wide dielectric relaxation which broadens and slows down on cooling.^{1,2} The relaxation originates from the dynamics of polar clusters, which develop below the Burns temperature $T_d \cong 620$ K.³ The broad distribution of relaxation frequencies has its origin in random fields and random forces as a consequence of chemical disorder in the perovskite B sites occupied by Mg^{2+} and Nb^{5+} . The local ferroelectric instability in the polar clusters was indicated by an unstable polar optic phonon, which softens to T_d and hardens above T_d .^{2,4} Although the dielectric properties of perovskite $\text{PbMg}_{1/3}\text{Nb}_{2/3}\text{O}_3$ were intensively studied during the last fifty years, not all is completely understood, particularly the complex and broad dielectric dispersion.

The related compound $\text{Pb}_{1.83}\text{Mg}_{0.29}\text{Nb}_{1.71}\text{O}_{6.39}$ (PMN) with a pyrochlore structure, which frequently grows in the perovskite PMN ceramics and thin films as a second phase and significantly deteriorates its dielectric properties, has been much less studied. The only report known to the authors is that by Shrout and Swartz.⁵ They investigated the dielectric response up to 400 kHz down to liquid He temperatures and observed a diffuse maximum in the complex permittivity below 40 K. The crystal structure of the pyrochlore PMN single crystal ($Fd3m$ space group) was determined in detail by Wakiya et al.⁶ High-frequency dielectric properties,

including microwave, THz and infrared frequencies, have not been investigated, although they could be useful for understanding the reported diffused and frequency dependent maximum of the complex permittivity. The present report aims to fill this gap in the literature. We will show that our pyrochlore PMN ceramics does not undergo a diffuse phase transition (reported in Ref.⁵), but a quantum paraelectric behavior for which the temperature dependent permittivity is caused only by anomalous polar phonons. In this way, it represents the first quantum paraelectrics with pyrochlore crystal structure.

II. EXPERIMENTAL

$\text{Pb}_{1.83}\text{Mg}_{0.29}\text{Nb}_{1.71}\text{O}_{6.39}$ pyrochlore ceramic samples were produced by solid state reaction of mixed oxide powders described in details in Refs.^{5,7}. PbO (99.5%), Nb_2O_5 (99.5%) and MgO (97%) powders were mixed and sintered at 880 °C for 8 hours. The pyrochlore cubic structure was verified by the X-ray diffraction.

The dielectric response was investigated between 400 Hz and 1 MHz from 10 K to 730 K using an impedance analyzer HP 4192A. The TE_{0n1} composite dielectric resonator method⁸ and network analyzer Agilent E8364B was used for microwave measurements at 8.8 GHz in 100 - 350 K temperature interval. The cooling rate was 2 K/min.

Measurements at terahertz (THz) frequencies from 7 cm^{-1} to 33 cm^{-1} (0.2 - 1.0 THz) were performed in the transmission mode using a time-domain THz spectrometer based on an amplified Ti - sapphire femtosecond laser system. Two ZnTe crystal plates were used to generate (by optic rectification) and to detect (by electro-optic sampling) the THz pulses. Both the transmitted field

amplitude and phase shift were simultaneously measured; this allows us to determine directly the complex dielectric response $\varepsilon^*(\omega)$. An Optistat CF cryostat with thin mylar windows (Oxford Inst.) was used for measurements down to 10 K.

Infrared (IR) reflectivity spectra were obtained using a Fourier transform IR spectrometer Bruker IFS 113v in the frequency range of 20 - 3000 cm^{-1} (0.6 - 90 THz) at room temperature, at lower temperatures the reduced spectral range up to 650 cm^{-1} only was studied (transparency region of polyethylene windows in the cryostat). Pyroelectric deuterated triglycine sulfate detectors were used for the room temperature measurements, while more sensitive liquid-He-cooled (1.5 K) Si bolometer was used for the low-temperature measurements. Polished disk-shaped samples with a diameter of 8 mm and thickness of ~ 2 mm were investigated.

III. RESULTS AND DISCUSSIONS

Temperature dependence of the real and imaginary parts of complex permittivity $\varepsilon^* = \varepsilon' - i\varepsilon''$ at various frequencies is plotted in Fig. 1. One can see typical incipient ferroelectric behavior, i.e. increase in ε' on cooling and its noticeable saturation at low temperatures. It is important to stress that within the accuracy of measurements no frequency dispersion of ε' was observed between 400 Hz and 8.8 GHz at temperatures below 600 K. The small low-frequency dispersion above 600 K is caused by non-negligible conductivity of our sample. The pronounced $\varepsilon'(T)$ dependence is therefore caused by the softening of an excitation above 10 GHz. To reveal it we measured the THz dielectric spectra (see Fig. 2) and IR reflectivity spectra (Fig. 3) below room temperature (RT). One can actually see very pronounced changes in the THz complex permittivity due to the polar phonon softening in the investigated range (see Fig. 2).

In order to obtain all phonon parameters as a function of temperature, IR and THz spectra were fitted simultaneously using the generalized-oscillator model with the factorized form of the complex permittivity:⁹

$$\varepsilon^*(\omega) = \varepsilon_\infty \prod_j \frac{\omega_{LOj}^2 - \omega^2 + i\omega\gamma_{LOj}}{\omega_{TOj}^2 - \omega^2 + i\omega\gamma_{TOj}} \quad (1)$$

where ω_{TOj} and ω_{LOj} denotes the transverse and longitudinal frequency of the j -th polar phonon, respectively, and γ_{TOj} and γ_{LOj} denotes their corresponding damping constants. $\varepsilon^*(\omega)$ is related to the normal reflectivity $R(\omega)$ by

$$R(\omega) = \left| \frac{\sqrt{\varepsilon^*(\omega)} - 1}{\sqrt{\varepsilon^*(\omega)} + 1} \right|^2. \quad (2)$$

The high-frequency permittivity ε_∞ resulting from the electron absorption processes was obtained from the room-temperature frequency-independent reflectivity

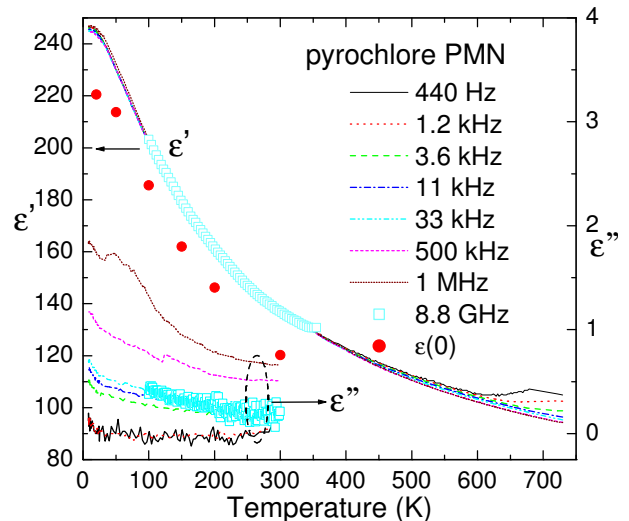


FIG. 1: (color online) Temperature dependence of the real ε' and imaginary ε'' part of complex permittivity in pyrochlore PMN ceramics at different frequencies. $\varepsilon(0)$ means the sum of phonon and electron contributions to the static permittivity, as obtained from the IR reflectivity and THz data fit. ε'' data are plotted only below 300 K, because its higher temperature values are influenced by the conductivity. Note the right scale for ε'' .

tails above the phonon frequencies and was assumed to be temperature independent.

The real and imaginary parts of $\varepsilon^*(\omega)$ obtained from the fits to IR and THz spectra are shown in Fig. 4. Parameters of the fits performed at 300 and 20 K are summarized in Table I. One can see a higher number of observed modes at 20 K than at RT. This is due to the reduced phonon damping at low temperatures, which allows to resolve a higher number of modes, which are probably overlapping at RT. One can see in the $\varepsilon''(\omega)$ spectra of Fig. 4 (we remind that the frequencies of ε'' maxima roughly correspond to the phonon frequencies) that the most remarkable frequency shift with temperature is revealed by the lowest frequency mode below 30 cm^{-1} , but also the mode near 130 cm^{-1} partially softens on cooling. The temperature dependence of the soft mode frequency ω_{SM} (left scale) and its dielectric strength $\Delta\varepsilon_{SM}$ are shown in Fig. 5. Mainly this mode causes an increase in ε' on cooling (see Fig. 1). In the case of uncoupled phonons the oscillator strength $f_j = \Delta\varepsilon_j \omega_{TOj}^2$ of each phonon is roughly temperature independent so that each softening of phonon frequency ω_{TOj} is connected with the increase of its dielectric strength $\Delta\varepsilon_j$ given by:⁹

$$\Delta\varepsilon_j = \varepsilon_\infty \omega_{TOj}^{-2} \frac{\prod_k \omega_{LOk}^2 - \omega_{TOj}^2}{\prod_{k \neq j} \omega_{TOk}^2 - \omega_{TOj}^2}. \quad (3)$$

In our case the soft-mode oscillator strength f_{SM} is temperature dependent, it increases twice from $3.3 \cdot 10^4$ to $6.5 \cdot 10^4 \text{ cm}^{-2}$. This indicates that the soft mode is coupled with some higher frequency mode assuming that

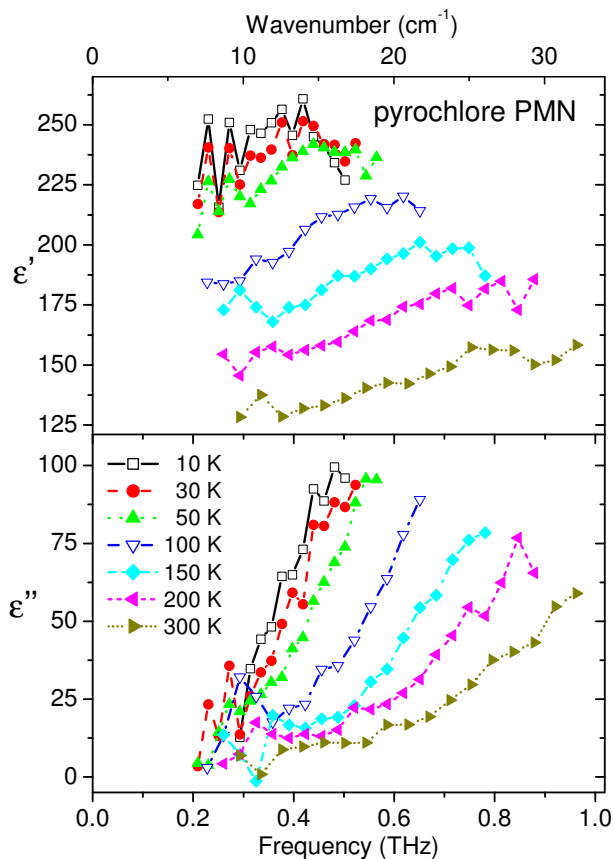


FIG. 2: (color online) THz dielectric spectra of the pyrochlore PMN at various temperatures. The soft mode frequency shifts down into the THz range on cooling, therefore the sample becomes less transparent at low temperatures (the noise increases) and the accessible spectral range narrows on cooling. Two frequency scales (THz and cm^{-1}) are given.

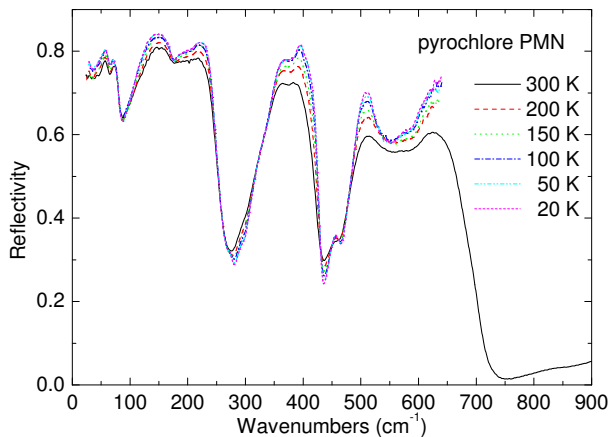


FIG. 3: (color online) IR reflectivity spectra of the pyrochlore PMN ceramics at various temperatures below RT. Low-temperature spectra were obtained only below 650 cm^{-1} (transparency range of the polyethylene windows in the cryostat).

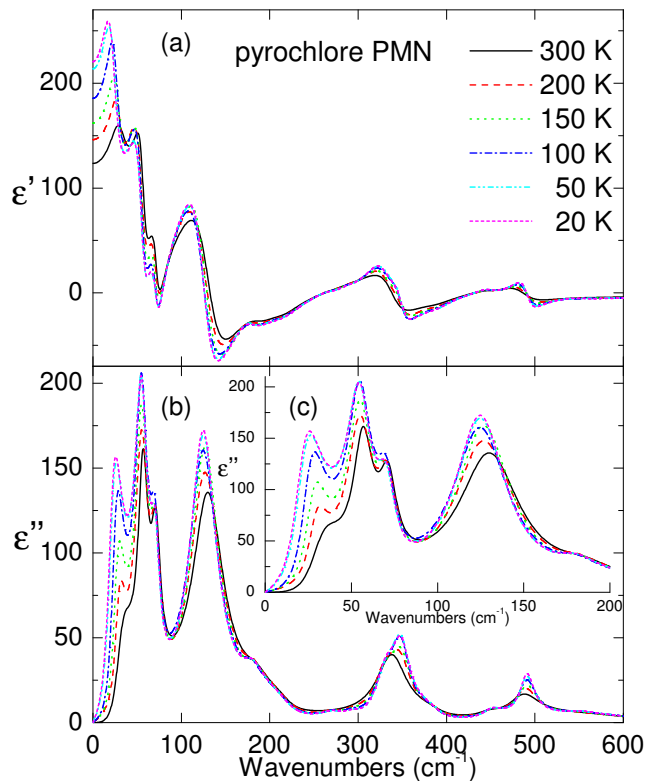


FIG. 4: (color online) Complex dielectric spectra from the fit to IR reflectivity and THz dielectric spectra at various temperatures. To see better the mode softening, $\epsilon''(\omega)$ in inset the spectra are shown in the spectral range below 200 cm^{-1} .

$\sum f_j = \text{const.}$ However, it is difficult to reveal with which mode is the soft mode coupled, because the oscillator strength of the most high-frequency modes is much higher than f_{SM} and relatively small changes (below the limit of our fitting accuracy) in these modes could explain the increase of the f_{SM} on cooling.

The static permittivity obtained from the fit of the IR reflectivity is defined as

$$\epsilon(0) = \sum_j \Delta\epsilon_j + \epsilon_\infty \quad (4)$$

and is plotted in Fig. 1 in red solid dots. The values of $\epsilon(0)$ are slightly lower (by about 20) than the experimental values obtained at and below the microwave range. However, we believe that the disagreement is rather due to the experimental inaccuracy than due to real dielectric dispersion above the GHz range. So we conclude that the temperature dependence of the permittivity below 10 GHz in Fig. 1 is essentially due to anomalous polar phonons.

The temperature dependence of the lowest-mode frequency below 35 cm^{-1} was fitted with the Cochran law

$$\omega_{SM}(T) = \sqrt{A(T - T_{cr})} \quad (5)$$

where A is a constant and T_{cr} is the critical softening

TABLE I: Parameters of the polar phonon modes in the pyrochlore PMN obtained from the fit of IR and THz spectra at 20 and 300 K. Frequencies ω_{TOj} , ω_{LOj} and dampings γ_{TOj} , γ_{LOj} of modes are in cm^{-1} , $\Delta\epsilon_j$ is dimensionless, $\epsilon_\infty=5.87$.

No	20 K					300 K				
	ω_{TOi}	γ_{TOj}	ω_{LOj}	γ_{LOj}	$\Delta\epsilon_j$	ω_{TOj}	γ_{TOj}	ω_{LOj}	γ_{LOj}	$\Delta\epsilon_j$
1	24.1	19.4	32.5	31.5	110.8	33.2	22.6	37.7	30.5	33.7
2	55.8	16.1	63.9	17.7	36.6	56.9	13.5	63.2	16.9	23.9
3	71.7	13.4	80.1	14.5	12.0	71.9	12.3	79.7	18.1	10.8
4	125.9	36.1	175.8	28.4	46.1	131.9	42.9	182.3	40.6	40.8
5	179.9	28.0	212.0	68.7	1.8	186.7	36.2	215.3	56.3	1.6
6	216.7	49.2	257.3	23.2	0.8	217.6	41.6	260.1	40.2	0.4
7	271.2	26.0	277.3	22.0	0.26					
8	293.5	23.7	296.0	22.0	0.2					
9	329.7	29.5	339.8	30.7	0.3					
10	348.9	23.7	388.1	49.2	2.0	338.8	41.1	383.5	48.9	4.3
11	389.1	36.6	429.5	20.6	0.06	386.5	40.8	427.7	32.4	0.2
12	449.6	28.1	464.1	33.6	0.3	448.4	31.7	456.3	35.0	0.2
13	490.9	19.9	547.6	59.5	0.9	486.3	41.9	530.7	116.5	1.0
14	547.8	43.4	551.2	55.6	0.001	553.1	120	586.1	120.4	0.4
15	562.6	44.8	575.1	70.7	0.9					
16	598.9	70.5	703.6	46.8	0.4	602.6	104.9	703.6	47.6	0.3
17	862.7	80.1	863.0	69.1	0.002	862.7	80.1	863	69.1	0.002

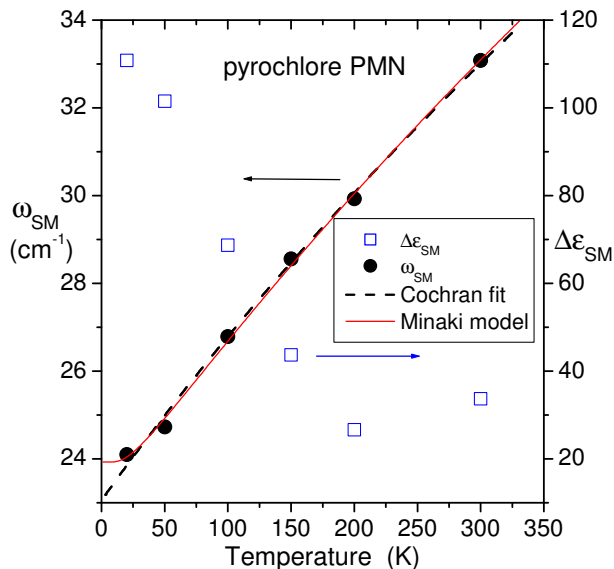


FIG. 5: (color online) Temperature dependence of the low-frequency soft mode ω_{SM} (left scale) and its dielectric strength (right scale). The dashed black line and solid red line show the results of the Cochran and Minaki fit of the soft-mode frequency, respectively (see the text).

temperature. From the fit we obtained $A = (1.86 \pm 0.01) \text{ cm}^{-2} \text{ K}^{-1}$ and $T_{cr} = (-285 \pm 11) \text{ K}$. So, pyrochlore PMN tends to the ferroelectric instability at negative temperatures.

Theoretical critical temperature can be obtained also

from the fit of the temperature dependence of permittivity $\epsilon(T)$, which (for classical paraelectrics) should follow the Curie-Weiss law

$$\epsilon' = \epsilon_{cw\infty} + \frac{C}{T - T_{cw}}. \quad (6)$$

The result of the Curie-Weiss fit is shown in Fig. 6 in dashed line with the following fit parameters: $\epsilon_{cw\infty} = 43 \pm 1$, Curie-Weiss constant $C = (47800 \pm 500) \text{ K}$ and critical temperature $T_{cw} = (-202 \pm 8) \text{ K}$. The Cochran critical temperature $T_{cr} = -285 \text{ K}$ is somewhat lower than the Curie-Weiss critical temperature T_{cw} , but if we consider that the extrapolated critical temperatures lie far below the investigated temperature range, the agreement between both values is reasonable.

The Curie-Weiss fit in Fig. 6 deviates from the experimental data below $\sim 50 \text{ K}$, because $\epsilon'(T)$ levels off at low temperatures. Similar behavior was observed in incipient ferroelectrics as SrTiO_3 , KTaO_3 or CaTiO_3 where the polar soft mode is also responsible for the observed $\epsilon'(T)$.^{10,11} The soft mode does not soften completely, it levels off at low temperatures (typically below 30 K), mainly due to zero-temperature vibrations of light oxygen ions, which prevents the formation of long-range ferroelectric order and permittivity divergence at low temperatures. Due to this phenomenon the incipient ferroelectrics are also called quantum paraelectrics.¹² Note that pyrochlore PMN is the first quantum paraelectrics of pyrochlore crystal structure.

The leveling-off of the low-temperature permittivity in incipient ferroelectrics was explained by Barrett¹³ al-

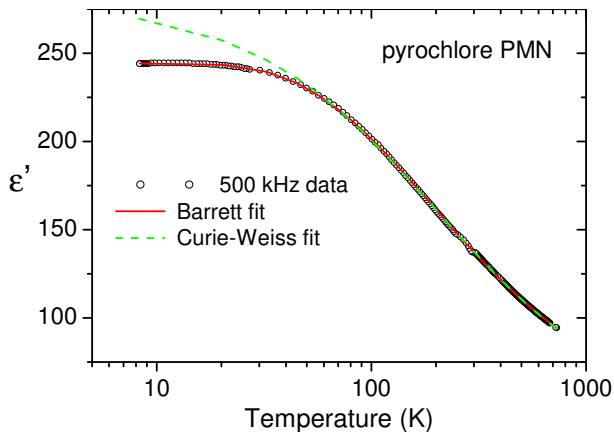


FIG. 6: (color online) The temperature dependence of the experimental permittivity at 500 kHz and result of the Curie-Weiss fit (dashed green line) and the fit with Barrett formula (red solid line). Note the log temperature scale.

ready in the beginning of 1950's. He derived the formula

$$\varepsilon'(T) = \frac{M}{\frac{T_1}{2} \coth\left(\frac{T_1}{2T}\right) - T_0} + \varepsilon_{B\infty}, \quad (7)$$

where M is constant, T_1 is the temperature below which the quantum fluctuations start to play a role ($\frac{1}{2}k_B T_1$ is the zero-point vibration energy¹⁴) and $\varepsilon_{B\infty}$ marks the temperature independent part of the permittivity (this term was neglected in Ref.¹³, because it was very small in comparison to huge low-temperature ε' in SrTiO₃ and KTaO₃). Our use of the Barrett formula in Eq.(7) for fitting of $\varepsilon'(T)$ yields very good agreement with the experimental data (see Fig. 6). We found $M=(4.25\pm 0.01)\times 10^4$ K, $T_1=(96\pm 8)$ K $T_0=(-167\pm 9)$ K and $\varepsilon_{B\infty} = 47\pm 0.5$. For $T \gg T_1$, $\frac{1}{2}T_1 \coth\left(\frac{T_1}{2T}\right)$ asymptotically approaches T and Eq.(7) becomes a Curie-Weiss law. Therefore also $\varepsilon_{B\infty} = 47$ is close to $\varepsilon_{CW\infty} = 43$. It is worth to note that the zero point vibration frequency $\frac{1}{2}k_B T_1 = 1$ THz = 33 cm⁻¹ corresponds very well to the soft mode frequency (see Fig. 5). Note also that the T_1 parameter as well as the soft-mode frequency in the pyrochlore PMN qualitatively agree with analogous parameters obtained for SrTiO₃ and SrTi¹⁸O₃, although the values of permittivity in these materials are two orders of magnitude higher,^{13,14,15} which is the consequence of different M parameters.

In the only published dielectric data below 400 kHz ShROUT and Swartz⁵ observed similar essentially dispersionless increase in ε' on cooling down to 50 K as we did in Fig. 1. We believe that the small dispersion below 50 K and small decrease in ε' below ~ 30 K observed by ShROUT and Swartz⁵ could be due to some defects (e.g. vacancies) in the crystal lattice of pyrochlore Pb_{1.83}Mg_{0.29}Nb_{1.71}O_{6.39}, which is substantially non-stoichiometric.

It is clear that the soft mode frequency cannot follow the Cochran law (Eq. 5) in the case of low-temperature

quantum fluctuations. The correct low-temperature dependence of the soft mode frequency derived from the Barrett formula for permittivity can be found e.g. in the paper of Minaki et al.¹⁶

$$\omega_{SM}(T) = \sqrt{A \left[\left(\frac{T_1}{2} \right) \coth\left(\frac{T_1}{2T} \right) - T_0 \right]}, \quad (8)$$

where A is constant and T_1 and T_0 have the same meaning as in Eq.(7). Note that Eq.(8) follows from Eq.(7) and Lyddane-Sachs-Teller relation under assumption that the temperature dependence of static permittivity is caused just by softening of the soft TO mode. Result of the soft mode fit with Eq.(8) is shown by solid line in Fig. 5 where one can clearly see the leveling-off of the soft-mode frequency at low temperatures (unlike the Cochran fit). The fitting parameters are the following: $A = (2.03\pm 0.05)$ cm⁻²K⁻¹, $T_1 = (96\pm 9)$ K and $T_0 = (-240\pm 11)$ K. The fit parameters could be significantly improved if we would have more points in Fig. 5 especially below 50 K. Nevertheless, one can see reasonable agreement of both Cochran and Barrett fits above 50 K as well as T_0 and T_1 parameters obtained from the Barrett fits of permittivity (Eq. 5) and the Minaki model of the soft mode frequency (Eq. 8).

Let us compare the IR reflectivity spectra of pyrochlore PMN (Fig. 3) with those of perovskite PMN. The latter was first published by Burns and Dacol³ together with the temperature dependence of the optical index of refraction $n(T)$, which shows deviation from the linear dependence below ~ 600 K. They explained the unusual $n(T)$ dependence by formation of polar nanoregions. Surprisingly, the published IR spectrum of the perovskite sample³ corresponds to our pyrochlore spectrum in Fig. 3. In later papers of other authors (Refs.^{17,18,19,20}) the mutually similar (but different from Burns and Dacol's spectra³) IR reflectivity spectra of perovskite PMN consisted of three distinct reflection bands typical for all cubic perovskite oxides. We stress that the infrared spectra in Refs.^{17,18,19,20} were obtained independently on ceramics, single crystals as well as on thin films. It appears that the IR spectrum by Burns and Dacol³ belongs to pyrochlore PMN. The rest of their data ($n(T)$ and $P(T)$) were obviously obtained on perovskite PMN, because the peculiarities near the Burns temperature in the perovskite PMN were later confirmed in many experiments.

It is of interest to compare the number of observed polar modes in the reflectivity spectra with the prediction of factor-group analysis: pyrochlore PMN crystallizes in $Fd3m$ space group with 8 formula units per conventional unit cell,⁶ i.e. 2 formula units per primitive unit cell. This means that on the whole, 66 lattice vibrational branches are expected. Pb ions are in 16d positions while Mg and Nb ions are in 16c positions⁶, both sites having D_{3d} symmetry, while the O cations are in positions 48f and 8b of C_{2v}^d and T_d symmetry, respectively. The mode symmetries and their activities in IR and Ra-

man spectra can be obtained using standard tables²¹ with the following result for the Γ -point of the Brillouin zone (factor-group analysis):

$$\begin{aligned} \Gamma_{Fd3m} = & 3A_{2u}(-) + 3E_u(-) + 8F_{1u}(x) + 4F_{2u} \\ & + 4F_{2g}(xy, yz, xz) + A_{1g}(x^2, y^2, z^2) \\ & + E_g(x^2 + y^2 - 2z^2, \sqrt{3}x^2 - \sqrt{3}y^2) + 2F_{1g}. \end{aligned} \quad (9)$$

It means that after subtraction of $1F_{1u}$ acoustic mode, $7F_{1u}$ modes should be IR active, $4F_{2g}$, $1A_{1g}$ and $1E_g$ should be Raman active, the rest of modes being silent. Table I shows that our fit of IR spectra required 17 modes, much more than expected. The analysis in Eq. 9 assumes one effective ion in 16c positions instead of statistically distributed Mg and Nb ions. Since the ions strongly differ in the mass, one could expect splitting of the modes in which these ions take part. If we take into account different Mg and Nb vibrations, the factor group analysis yields:

$$\begin{aligned} \Gamma_{Fd3m} = & 4A_{2u}(-) + 4E_u(-) + 10F_{1u}(x) + 5F_{2u} \\ & + 4F_{2g}(xy, yz, xz) + A_{1g}(x^2, y^2, z^2) \\ & + E_g(x^2 + y^2 - 2z^2, \sqrt{3}x^2 - \sqrt{3}y^2) + 2F_{1g}. \end{aligned} \quad (10)$$

In this case 9 polar F_{1u} modes are expected, which is still less than 17 modes observed at low temperature (see Table I). If we assume that the Pb cations and some of the oxygen anions are dynamically disordered among more equivalent positions with the average structure remaining cubic like in isostructural $\text{Bi}_{1.5}\text{ZnNb}_{1.5}\text{O}_7$,²² then 14 modes could be IR active,²³ close to our experimental result.

The problem with the excess IR active modes is also known from the perovskite PMN, where only $4F_{1u}$ polar modes are allowed in $Fm\bar{3}m$ structure, although 7 modes were observed.¹⁹ The excess modes in the perovskite PMN were explained by polar clusters, which locally break the cubic symmetry into a rhombohedral one.²⁰ In the case of pyrochlore structure similar local symmetry breaking, if present, should probably be non-polar, because there is no indication for the existence

of polar clusters. There is also no dielectric dispersion below the polar phonon range, in contrast to the PMN perovskite, where the huge dielectric dispersion appears just due to polar cluster dynamics.^{1,2} Therefore it appears that new structural studies of pyrochlore PMN are needed to detect either a dynamical disorder of some atoms in the lattice or a non-cubic crystal symmetry.

IV. CONCLUSION

Our dielectric studies of pyrochlore PMN indicate quantum paraelectric behavior, i.e. the permittivity increase on cooling following the Barrett formula in the whole investigated temperature range. The permittivity shows no dispersion up to the microwave range and its temperature dependence can be explained by the softening of polar optic modes. The zero-point vibrational energy $\frac{1}{2}k_B T_1 = 1$ THz obtained from the Barrett formula corresponds very well to the soft mode frequency observed near 30 cm^{-1} . It is worth to note that the pyrochlore PMN is the first quantum paraelectrics with pyrochlore crystal structure. Our IR spectrum of pyrochlore PMN corresponds to IR spectrum by Burns and Dacol³, whose paper concerns the perovskite PMN. By comparing it with the later results,^{17,18,19,20} it becomes clear that Burns and Dacol published (by mistake) the IR spectrum of the pyrochlore PMN. Since the IR experiment revealed more modes than expected from the factor-group analysis, we suggest that the structure should have at least locally lower symmetry than the cubic one.

Acknowledgments

The work has been supported by the Grant Agency of the Czech Republic (Project No. 202/06/0403) and AVOZ10100520.

* Electronic address: kamba@fzu.cz

¹ D. Viehland, M. Wuttig, and L.E. Cross, *Ferroelectrics* **120**, 71 (1991).

² V. Bovtun, S. Veljko, S. Kamba, J. Petzelt, S. Varkhrushev, Y. Yakymenko, K. Brinkman, and N. Setter, *J. Eur. Ceram. Soc.* **26**, 2867 (2006) and references therein.

³ G. Burns and F. H. Dacol, *Solid State Commun.* **48**, 853 (1983).

⁴ S. Wakimoto, C. Stock, Z.-G. Ye, W. Chen, P. M. Gehring, and G. Shirane, *Phys. Rev. B* **66**, 224102 (2002).

⁵ T. R. ShROUT and S. L. Swartz, *Mat. Res. Bull.* **18**, 663 (1983).

⁶ N. Wakiya, A. Saiki, N. Ishizawa, K. Shinozaki, and N. Mizutani, *Mat. Res. Bull.* **28**, 137 (1993).

⁷ A. Mergen and W.E. Lee, *J. Eur. Ceram. Soc.* **17**, 1033 (1997).

⁸ J. Krupka, T. Zychowicz, V. Bovtun, S. Veljko, *IEEE Trans. UFFC* **53**, 1883 (2006).

⁹ F. Gervais, in *Infrared and Millimeter Waves*, vol. 8, ed. K. J. Button (New York: Academic) chapter 7, p. 279.

¹⁰ G. A. Samara, *Solid State Physics, Advances in Research and Applications*, Vol. 56. San Diego: Academic Press, pp. 240-458 (2001) and references therein.

¹¹ O.E. Kvyatkovskii, *Phys. Solid State* **43**, 1401 (2001) and references therein.

¹² K. A. Müller and H. Burkard, *Phys. Rev. B* **19**, 3593 (1979).

¹³ J.H. Barrett, *Phys. Rev.* **86**, 118 (1952).

- ¹⁴ W. Kleemann and J. Dec, *Phys. Rev. B* **75**, 027101 (2007).
- ¹⁵ C. Filipic and A. Levstik, *Phys. Rev. B* **73**, 092104 (2006).
- ¹⁶ Y. Minaki, M. Kobayashi, Y. Tsujimi, T. Yagi, M. Nakanishi, R. Wang, and M. Itoh, *J. Korean Phys. Soc.* **42**, S1290 (2003).
- ¹⁷ A. A. Karamyan, *Sov. Phys. Solid State* **18**, 1861 (1977).
- ¹⁸ I. M. Reaney, J. Petzelt, V. V. Voitsekhovskii, F. Chu, and N. Setter, *J. Appl. Phys.* **76**, 2086 (1994).
- ¹⁹ S.A. Prosandeev, E. Cockayne, B.P. Burton, S. Kamba, J. Petzelt, Yu. Yuzyuk, R.S. Katiyar, and S.B. Vakhrushev, *Phys. Rev. B* **70**, 134110 (2004).
- ²⁰ J. Hlinka, T. Ostapchuk, D. Noujni, S. Kamba, and J. Petzelt, *Phys. Rev. Lett.* **96**, 027601 (2006).
- ²¹ D.L. Rousseau, R.P. Bauman, and S.P.S. Porto, *J. Raman Spectr.* **10**, 253 (1981).
- ²² I. Levin, T.G. Amos, J.C. Nino, T.A. Vanderah, C.A. Randall, and M.T. Lanagan, *J. Sol. State Chem.*, **168**, 69 (2002).
- ²³ S. Kamba, V. Porokhonsky, A. Pashkin, V. Bovtun, J. Petzelt, J.C. Nino, S. Trolier-McKinstry, M. T. Lanagan, and C.A. Randall, *Phys. Rev. B* **66**, 054106 (2002).